

1 **Time-dependent Coulomb stress changes induced by the 2002-2003 Etna magmatic intrusions**
2 **and implications on following seismic activities**

3

4

5 Fabio Pulvirenti¹, Marco Aloisi² and Shuanggen Jin¹

6 ¹ Shanghai Astronomical Observatory, Chinese Academy of Sciences, Shanghai, China

7 ² Istituto Nazionale di Geofisica e Vulcanologia, Osservatorio Etneo, Catania, Italy

8 Email: fabiopulvirenti@yahoo.it (F. Pulvirenti); marco.aloisi@ingv.it (M. Aloisi);

9 sgjin@shao.ac.cn (S. Jin) ;

10

11 **Abstract**

12

13 In this paper, the relationship between the dike-forming magmatic intrusions and the faulting
14 process at Mount Etna is investigated in terms of Coulomb stress changes. As case study, a
15 complete time-dependent 3-D finite element model for the 2002-2003 eruption at Mount Etna is
16 presented. In the model, which takes into account the topography, medium heterogeneities and
17 principal fault systems in a viscoelastic/plastic rheology, we sequentially activated three dike-
18 forming processes and looked at the induced temporal evolution of the Coulomb stress changes,
19 during the co-intrusive and post-intrusive periods, on Pernicana and Santa Venerina faults. We
20 investigated where and when fault slips were encouraged or not, and consequently how earthquakes
21 may have been triggered. Results show positive Coulomb stress changes for the Pernicana Fault in
22 accordance to the time, location and depth of the 27th October 2002 Pernicana earthquake ($M_d =$
23 3.5). The amount of Coulomb stress changes in the area of Santa Venerina Fault, as induced by
24 dike-forming intrusions only, is instead almost negligible and, probably, not sufficient to trigger the
25 29th October Santa Venerina earthquake ($M_d = 4.4$), occurred two days after the start of the

1 eruption. The necessary Coulomb stress change value to trigger this earthquake is instead reached if
2 we consider it as induced by the 27th October Pernicana biggest earthquake, combined with the
3 dike-induced stresses.

4

5 Keywords: Coulomb stress changes; Finite Element Model; Viscoelasticity; Earthquakes; Mount
6 Etna

7

8 **1. Introduction**

9

10 One of the most challenging problems in studying the tectonic deformations is to understand the
11 conditions under which rock fails along the fault planes and how the fault movements are related
12 each other. These relationships can be investigated by the estimated stress changes along the faults
13 before and after the earthquakes. At Mount Etna, the stress, triggered by the push of the dike-
14 forming intrusions, together with the regional compressive regime, is transferred to the faults and
15 redistributed among them [e.g., Patanè et al., 2005; Feuillet et al., 2006; Mattia et al., 2007; Currenti
16 et al., 2008a; Aloisi et al., 2011; Bonanno et al., 2011; Privitera et al., 2012; Gonzalez and Palano,
17 2014]. In particular, Feuillet et al. [2006], after analyzing historical earthquakes in eastern Sicily
18 and eruptions at Mt Etna volcano, clearly found that volcanic sources and active faults, located
19 nearby the volcano, are mechanically coupled, and therefore they can interact each other by
20 changing or perturbing the stress state and, in turn, promoting or inhibiting earthquakes or
21 eruptions.

22 If earthquakes occur, the stress state of the medium is modified by an additional stress field
23 [e.g., Dragoni et al., 1982; Privitera et al., 2012]. The stress changes depend on fault location,
24 geometry and sense of slip (rake). It is commonly referred to stress changes as Coulomb stress
25 changes, hereafter CSC. The importance of the CSC in imaging the areas of stress transfer among
26 faults has been widely demonstrated in many works [e.g., Thatcher and Savage, 1982; Harris et

1 al., 1992; Jaumé and Sykes, 1992; Reasenbergs and Simpson, 1992; King et al., 1994; Gross and
2 Kisslinger, 1997; Harris, 1998; Nostro et al., 1998; Vidale et al., 1998; Stein, 1999; Hill et al.,
3 2002; Marzocchi et al., 2002; Toda et al., 2002; Hyodo and Hirahara, 2004; Walter and Amelung,
4 2004; Feuille et al., 2006; Calais et al., 2010; Toda et al., 2011]. The estimated stress increases are
5 rarely more than a few bars (1 bar, which is approximately atmospheric pressure at sea level), or
6 just a few percent of the mean earthquake stress drop [Stein, 1999]. The CSC quantity [bar] can be
7 regarded as an alteration of the “potentiality” of slip of the fault plane in response to the current
8 stress state of the medium [Kilb et al., 2000]. If this quantity is positive (or negative), the movement
9 on the fault plane is encouraged (or discouraged) and earthquakes can be generated (or not).
10 Incorporating, as we here made, the viscoelastic effects that modify the Coulomb stress with time,
11 the variation of the stress changes in space and time through the lithosphere can give information on
12 the arrival of a “stress wave” [e.g., Pollitz and Sacks, 1997; Freed and Lin, 1998; Kenner and
13 Segall, 1999; Sevilgen et al., 2012] on a seismogenetic structure, this “wave” might then trigger an
14 earthquake in this zone, if the right conditions (depending on rheology, friction and connection
15 between crustal discontinuities) are found. Moreover, the stress distribution among the faults can be
16 used to investigate the relation between the mainshock on a fault and the probability of aftershocks
17 in the nearby faults. The strong concentration of aftershocks found at the site of such small stress
18 increases is explained in terms of rupture nucleation phenomena, observed in laboratory [Stein,
19 1999].

20 The minimum positive value of CSC to trigger an earthquake depends on the area where the
21 fault is located because of the different rheological conditions. In the Etnean area, changes much
22 lower than 1 bar are considered usually sufficient to trigger movements on the fault plane [Bonanno
23 et al., 2011; Privitera et al., 2012; Gonzalez and Palano, 2014]. In some areas, aftershocks can be
24 triggered even when the stress is increased by about 0.3 bar [Toda et al., 2011]. Many authors [e.g.,
25 Harris et al., 1992; Jaumé and Sykes, 1992; Reasenbergs and Simpson, 1992; Gross and Kisslinger,
26 1997; Stein, 1999; Bonanno et al., 2011; Privitera et al., 2012] reported that static stress changes

1 greater than or equal to 0.1 [bar] may trigger seismicity within a rock volume, close to the critical
2 state of failure. For example, it was found that 67% of the 10,000 $M > 1$ Landers (California, 1992,
3 $M_w = 7.3$) aftershocks occurred in regions calculated to have been brought >0.1 bar closer to failure
4 and few aftershocks occurred in regions inhibited by >0.1 bar from failure (stress shadows), [Stein,
5 1999]. Anderson and Johnson [1999] obtained that aftershocks of the 1987 ($M_w = 6.6$) sequence at
6 Superstition Hills (California) show significant correlations for stress increases >0.1 bar during 1.4-
7 2.8 yr after the mainshock. An earthquake, producing weak stress increases, can thus enhance or
8 suppress subsequent events, depending on their location and orientation. Viewed in this light,
9 aftershocks are simply sites of seismicity rate increase, occurring where the stress has increased
10 [Stein, 1999]. Some authors retain that the CSC lower limit, for a significant correlation between
11 seismicity rate change and static stress changes, could be considered equal to the value produced by
12 tides (about 0.01 bar). In fact, Vidale et al. [1998] found that, along the creeping portions of the San
13 Andreas and Calaveras faults, the rate of seismicity during the peak tidal unclamping is 1.0% higher
14 than average. Thus, even tides can perceptibly alter the rate of seismicity, suggesting that the much
15 larger stress changes associated with earthquakes are indeed one cause of seismicity rate changes.
16 Therefore, a significant lower limit for the CSC can be considered as equal to about 0.1 bar.
17 Moreover, seismic waves [e.g., Stein, 1999; Cai, 2001; Resende et al., 2010; Palaniyandi Kamatchi
18 et al., 2013] excited by earthquakes produce dynamic CSC that, at distances more than about one
19 source dimension from the fault, can be an order of magnitude larger than the, here discussed, static
20 stress changes. Since the transient stress oscillate, stress changes are everywhere positive and,
21 therefore, dynamic stresses should produce no seismicity rate decreases, at odds with observations
22 [Stein, 1999]. Therefore, exclusively the weak permanent stress changes should control the
23 seismicity. Alternatively, some authors [e.g., Kilb et al, 2000] found that dynamic stresses alter the
24 mechanical state or properties of the fault zone and these dynamically weakened faults may fail
25 after the seismic waves have passed.

1 In this paper, the relationship between the dike-forming magmatic intrusions and the faulting
2 process at Mount Etna is investigated in terms of static CSC. The model is developed using the
3 commercial software COMSOL Multiphysics [<https://www.comsol.com/>] and it is an improvement
4 of a previous 3D finite element model [Aloisi et al., 2011]. In particular, considering the analysis of
5 the spatial-temporal evolution of the epicentral pattern during the period of 26-29 October 2002 as
6 described in [Barberi et al., 2004] and [Palano et al., 2009], we used the equations described in
7 Piombo et al. [2007] for shear and tensile dislocations in a viscoelastic halfspace, adapting them for
8 heterogeneities, where the viscoelastic areas are described by a generalized Maxwell model. We
9 included also a plastic layer representing the ductile carbonates substrate corresponding to the
10 Hyblean Plateau [Heap et al., 2013; Bakker et al., 2015]. It is noteworthy that long-lived magma
11 bodies are present at depths corresponding to the Hyblean Plateau [e.g., Chiarabba et al., 2000] that
12 starts at about a depth of 5 km underneath the volcanic edifice and has an average thickness of
13 about 10 km. Therefore, the involvement of the Hyblean Plateau with the magmatic plumbing
14 system at Mt. Etna volcano, potentially exposes fresh and unaltered carbonate rock to high
15 temperatures [Heap et al., 2015]. Thermal-stressing results in a progressive and significant change
16 in the physical properties of the rocks [Heap et al., 2015]. Inside this FEM model, we activated
17 sequentially (in a time-dependent manner) each dike-forming process, whose size and position has
18 been evinced by previous calculations [see Aloisi et al., 2011]. Since the sequential activation of the
19 dike-forming processes induces a variation in the CSC, which can be monitored with respect to the
20 time [Pollitz and Sacks, 1997; Freed and Lin, 1998; Kenner and Segall, 1999; Toda et al., 2002;
21 Sevilgen et al., 2012], we looked at the temporal effect of the dike-forming intrusions on Pernicana
22 and Santa Venerina faults, which were reactivated during the eruption period. In particular, we
23 looked at the temporal variation of the CSC in relation to two seismic events, the 27th October 2002
24 01:28 GMT Pernicana earthquake ($M_d = 3.5$) and the 29th October 10:02 GMT Santa Venerina
25 earthquake ($M_d = 4.4$), see Figure 1. The evolution of the CSC in the eastern flank during the 26-29
26 October 2002 was investigated through the following two phases: a) in the first phase (26-27

1 October 2002), we looked at the temporal CSC evolution on the Pernicana Fault plane, in order to
2 see if the stress changes induced by the magmatic intrusions were temporally and spatially
3 correlated with the 27th October earthquake, where the Pernicana Fault was treated as a “passive”
4 (receiving) fault; b) in the second phase (27-29 October 2002), we looked at the CSC on Santa
5 Venerina Fault plane. In this latter case, we evaluated the separate stress changes effect due to the
6 dike-forming intrusions only and, then, to a combination of dike-forming intrusions plus an “active”
7 left-lateral strike slipping Pernicana Fault (western segment), whose movement of several
8 centimeters has been evinced by geological surveys during the eruption period [Neri et al., 2004;
9 2005]. In this case, Pernicana Fault is additionally displaced in order to consider the effect of the
10 pre-stress produced by the action of previous intrusive phenomena [Neri et al., 2004; Bonforte et
11 al., 2007b; Puglisi et al., 2008; Currenti et al., 2012; Alparone et al., 2013a and 2013b; Ruch et al.,
12 2013]. We obtained that the dike-forming intrusions are responsible for the activation of Pernicana
13 fault. Moreover, the earthquake on Pernicana fault, combined with the dike-induced stresses, may
14 have triggered the earthquake on Santa Venerina fault.

15 In the followings, the Mount Etna tectonics and model settings are shown in Sections 2 and 3,
16 results and discussions are presented at Section 4, and finally conclusions are given in Section 5.

17

18 **2. Tectonic setting and the 2002-2003 eruption**

19

20 Mount Etna is a basaltic strato-volcano located in the eastern coast of Sicily (Italy) along the
21 front of the collision belt between the African and the Eurasian plates and at the footwall of the
22 Malta Escarpment (a major normal fault system separating the Hyblaean foreland from the thinned
23 Ionian crust, Fig. 1). The volcano is subject to an about N-S striking compressive regime due to the
24 convergence between the two plates [e.g., Cocina et al., 1997; Barberi et al., 2000] and to an
25 extensional, about WNW-ESE, regime, associated to the Malta Escarpment dynamics [e.g., Ellis
26 and King, 1991; Hirn et al., 1997]. Together with the two previous described stress regimes, the

1 volcanic edifice is subject to local stress due to magma activities [e.g., Barberi et al., 2000]. The
2 analysis of the distribution of the GPS velocity vectors during the inflation and deflation periods
3 suggests that the volcanic edifice can be described as characterized by two kinematically distinct
4 sectors: the western flank that has a scant morphological evidence of faulting or eruptive fracturing
5 and is buttressed to the western and northern part by the Maghrebian Chain, and the eastern flank
6 that is formed by several fault systems accommodating a near constant seaward flank displacement
7 whose origin is still lively debated [for a comprehensive excursus see, e.g., Palano et al., 2008;
8 Palano et al., 2009; Aloisi et al., 2011; Chiocci et al., 2011; Cannavò et al., 2014].

9 There are principally two types of eruptions at Etna [e.g., Aloisi et al., 2009]: a) summit
10 strombolian eruptions, where magma intrudes through the central conduit, and b) dike-forming
11 eruptions that can be lateral (when magma departs horizontally from the central conduit to reach the
12 volcano flank) or eccentric (when magma propagates vertically from several kilometers depth to
13 break out at the surface bypassing the central conduit system). Most of dike-forming intrusions
14 ascend along two rift zones, a) the NE Rift, which is an about 5 km long, 1 km wide, topographic
15 ridge extending between 2500 m and 1850 m (above sea level - hereafter, a.s.l.), made up of lavas
16 and pyroclastics, and b) the S Rift zone, a diffuse set of NNW-SSE to SSW-NNE striking fissures,
17 which extends down to Nicolosi village and is marked by aligned spatter cones coalesced at places
18 to the volcanic ridges (Fig. 1).

19 Previous studies argued that the 2002 magma intrusion mechanically interacted with pre-
20 existing structures (Northeast Rift and Pernicana Fault), which influenced the stress propagation
21 and were reactivated during dike intrusions [e.g., Acocella et al., 2003; Del Negro et al., 2004;
22 Walter et al., 2005; Currenti et al., 2007; Aloisi et al., 2011]. Moreover, the close correlation
23 between seismic activities and magmatic intrusions was provided by previous studies (e.g.,
24 Bonforte et al., 2007a; Currenti et al., 2010), which affirmed that the dynamics of Mt. Etna in the
25 summer of 2002 resulted in optimal conditions for the onset of the 2002-2003 eruption, referring, in
26 particular, to the 22 September 2002 ($M_d = 3.7$) earthquake that struck the northeastern part of Mt.

1 Etna and to a consequent tensile mechanism that was detected in the upper part of the Pernicana
2 Fault and was interpreted as a precursor of the eruption that occurred a month later.

3 The work, here presented, focused on better understanding the described relations between the
4 dike-forming intrusions and the principal fault systems, activated during the 2002-2003 eruption,
5 which is one of the best studied events ever at Mount Etna [e.g., Del Negro et al., 2004; Andronico
6 et al., 2005; Neri et al., 2005; Andronico et al., 2008; Currenti et al., 2008b; Spampinato et al.,
7 2008; Ferlito et al., 2009; De Gori et al., 2011; Steffke et al., 2011], being characterized by diffuse
8 ground fracturing [Neri et al., 2004; Neri et al., 2005], strong explosive activity and
9 petrographically distinct lava outputs and so suitable for the proposed investigation.

10 The 2002-2003 eruption started late on the night of the 26 October 2002, heralded by only a
11 few hours of premonitory seismicity. After fourteen months of repose succeeding the eruption of
12 July-August 2001, at 20:12 UTC on 26 October 2002, a seismic swarm indicated the beginning of a
13 new eruptive episode. During the first 3-4 hours, it took place in the southern-upper part of the
14 volcano [Barberi et al., 2004]. A ground-based thermal survey, carried out at 4:00:05 UTC on the
15 27th, revealed the opening of eruptive fissures on the volcano's southern flank [Spampinato et al.,
16 2008]. A first dike-forming intrusion ascended vertically through the volcano edifice (Fig. 1 and 2)
17 in only a few hours and was located south of the summit area (South Rift), close to the 2001
18 eruption site [Bonaccorso et al., 2002; Aloisi et al., 2003; Aloisi et al., 2006]. On 27 October, a
19 second dike-forming intrusion propagated laterally along the NE Rift (Fig. 1 and 2) for a few days
20 [Aloisi et al., 2006]. The NE intrusion, active for nine days, demonstrated prevalent strombolian
21 activity, producing a lava volume of about $8-12 \cdot 10^6 \text{ m}^3$ [Andronico et al., 2005]. The southern
22 activity lasted a total of 81 days and was characterized by high explosive and minor effusive
23 activity, that produced a flow field of about $25-34 \cdot 10^6 \text{ m}^3$. Fire fountaining formed sustained
24 eruptive columns and caused abundant tephra fallout whose volume has been estimated to be 43 ± 6
25 $\cdot 10^6 \text{ m}^3$ [Andronico et al., 2008].

1 The double intrusions were preceded, accompanied and followed by intense seismic activity
2 (874 earthquakes, $M_d \geq 1$, during the whole period), [Barberi et al., 2004; Gambino et al., 2004;
3 Monaco et al., 2005; Neri et al., 2005; De Lorenzo et al., 2010]. In particular, most of the seismic
4 energy was released during the first four days (470 events on a total of 874, $M_{\max} = 4.4$). Before the
5 onset of the eruption, at 20:25 (GMT) on October 26, 2002 and until 01:28 GMT on 27 October, a
6 seismic swarm took place in the central upper part of Mt. Etna. Successively, the epicentral seismic
7 pattern showed a northeastward migration of earthquakes along the NE Rift [Aloisi et al., 2006]. In
8 the early morning of 27 October, seismicity (01.28 GMT, depth = 1.6 km above the sea level
9 (a.s.l.), $M_d = 3.5$; left lateral motion) involved also the western tip of the WNW-ESE trending
10 Pernicana Fault on the northeastern flank of the volcano, destroying the Piano Provenzana skiing
11 station [Gruppo Analisi Dati Sismici, 2014; Alparone et al., 2015]. Two days later, on the eastern
12 flank, the Timpe fault system was reactivated with dextral-oblique motion in the area of the Santa
13 Venerina Fault (10.02 GMT, depth = 0.7 km below the sea level (b.s.l.), $M_d = 4.4$; 16.39 GMT,
14 depth = 2.8 km b.s.l., $M_d = 4.0$; 17.14 GMT, depth = 2.2 km b.s.l., $M_d = 4.1$) [Monaco et al., 2005].
15 Moreover, aseismic slip along the San Gregorio-Acitrezza Fault also occurred after the Timpe
16 seismic sequences [Monaco et al., 2011]. On 29 October, after a decrease in the earthquake rate, a
17 sharp resumption due to the activation of new seismic structures in south-eastern flank was
18 observed [Monaco et al., 2005]. The eruption ended on January 28, 2003.

19 The deformation pattern recorded during the 2002–2003 eruption was extensively analyzed by
20 analytical [e.g., Aloisi et al., 2003, 2006; Bonforte et al., 2007b] and numerical modelling [e.g.,
21 Walter et al., 2005; Currenti et al., 2008a, 2010; Aloisi et al., 2011]. The models indicated that the
22 observed displacements can be interpreted as the response of the volcanic edifice to a pair of dike-
23 forming intrusions: a rapid ascent of an eccentric dike-forming intrusion that triggered the eruption
24 in the southern flank and a lateral intrusion of a second dike-like body in the north-eastern flank
25 (Fig. 1 and 2).

26

1 **3. Model settings**

2

3 The numerical model presented in this work is an improvement of the analysis performed in
4 Aloisi et al. [2011] and has been developed with the commercial software COMSOL Multiphysics.
5 The model takes into account the topography, the medium heterogeneities, the most active crustal
6 discontinuities, with specified friction coefficients, and the magmatic sources related to the 2002-
7 2003 Etna eruption, described as a set of tabular dislocations [Aloisi et al., 2011], Figures 1 and 2.
8 We first verified that the dimension of FEM domain was large enough to cancel out any
9 displacements in proximity to the external boundaries, avoiding the generation of artifacts on the
10 solution [Aloisi et al., 2011]. Moreover, with the aim of verifying if near field displacements were
11 reproduced with an acceptable accuracy in our numerical domain, we performed a comparison
12 between numerical and analytical displacements produced by the three tabular dislocations,
13 obtaining a standard deviation between the two solutions, on the free surface, of few millimeters
14 (0.003 m). In terms of material characterization, the novelty, with respect to the model developed in
15 Aloisi et al. [2011], is the inclusion of a viscoelastic and of a plastic domain which allow looking at
16 coseismic and postseismic deformations along Pernicana and Santa Venerina faults in a more
17 realistic manner. Viscoelasticity at Mount Etna is motivated by the displacements recorded at
18 Pernicana Fault. In fact, results from post-intrusive GPS monitoring with five months encompassing
19 and following the onset of 2002-03 Mt. Etna eruption showed that, after the end of the northern
20 intrusion, the Pernicana Fault continued to slip and the overall ground deformation pattern may be
21 explained in terms of a time-dependent viscoelastic relaxation process or using an after-slip
22 mechanism [Palano et al., 2009]. Either proposed model may explain the observed time-dependent
23 deformation. In volcanic areas, rocks near magmatic sources are considerably heated and
24 viscoelastic relaxation is a mechanism commonly invoked to explain postseismic stress field
25 changes [e.g., Newman et al. 2001; Freed and Lin, 2001; Currenti et al., 2008b]. In our work, we
26 evaluated the viscoelastic relaxation approach. In particular, the post-intrusive deformation

1 observed at surface could have been driven by viscoelastic flow, in a weak layer encompassing the
2 clayey sedimentary basement and located below an elastic layer, in response to the stress
3 concentration. We think that this idea is reliable because is compatible with the presence of the
4 about 1 km thick clay layer under the volcanic edifice and of incoherent clay material outcropping
5 along Pernicana Fault together with volcanic rocks, which lowers the viscosity of the lithosphere
6 (usually $\sim 10^{17} - 10^{20}$ Pa*s; Hearn et al., 2002; Hearn, 2003; Sheu and Shieh, 2004). Palano et al.
7 [2009] found values of viscosity for this area ranging between $\sim 7.1 \times 10^{14} - 1.3 \cdot 10^{15}$ Pa*s, lower
8 than those estimated (6.1×10^{16} Pa*s for a relaxation time of 3.5 years) for the relaxation of the
9 basaltic substrate [Briole et al., 1997]. It is noteworthy that, Pavlov [1960] obtained viscosity values
10 of about 10^{13} Pa*s for several low melting clays.

11 Moreover, in active volcanic zones, magmatic activity, heating the surrounding rocks, perturbs
12 the geothermal gradient at relatively shallow crustal level, beyond the brittle-ductile transition
13 temperature. Therefore, heated and weakened rocks at shallow levels, above ~ 5.0 km (b.s.l.), no
14 longer behave in a purely elastic manner [Del Negro et al., 2009]. Worldwide, the interval from
15 ~ 1.5 km to ~ 4.0 km (b.s.l.) represents, a region of neutral buoyancy where magma densities and
16 country rock densities are just balanced [e.g., Ryan, 1987, 1993, 1994; Corsaro and Pompilio,
17 2004]. In the last decade, for Etna volcano, many active magmatic sources have been found in
18 correspondence of this zone of neutral buoyancy [e.g., Aloisi et al., 2011; Bruno et al., 2012], along
19 the magma pathways historically resolved by GPS, seismic and other geophysical data (see Aloisi et
20 al. [2011]), bounding a high v_p body [e.g., Aloisi et al., 2002; Patanè et al., 2006]. By following
21 these considerations, we considered (Fig. 2) a viscoelastic layer maximum depth of 3 km (b.s.l.),
22 which is compatible with the depth of the neutral buoyancy level (from ~ 1.5 km to ~ 4.0 km, b.s.l.)
23 and the depth of the above lying clayey substratum (~ 1 km thick), including the discontinuously
24 outcroppings along Pernicana Fault and in the eastern flank [Branca and Ferrara, 2001; Bonforte et
25 al., 2007a].

1 It is noteworthy that, as showed in Singh and Roseman [1974] and for a vertical strike-slip
 2 rectangular fault, the results in using viscoelastic models differ significantly from the corresponding
 3 elastic results. According to the above considerations, the application of a viscoelastic rheology
 4 could allow us to obtain a model that better approximate the observed behaviour of the volcano.
 5 Therefore, we here developed a time-dependent model.

6 In our model, the viscoelastic behaviour of the medium is represented by using a generalized
 7 Maxwell model [e.g., Trasatti et al., 2003; Del Negro et al., 2009], with two spring-dashpot
 8 elements. The model is characterized by a shear modulus G_0 , as a function of the Young's modulus
 9 and the Poisson's ratio, deduced by the seismic tomography of Aloisi et al. [2002], Figure 2.
 10 Therefore, our domain is inhomogeneous and anisotropic. The fractional shear moduli μ_1 and μ_2 of
 11 the two branches, have the same value, equal to 0.5 [Del Negro et al., 2009], however the related
 12 relaxation times for each branch are different. This means that even if the viscosity of the dashpots
 13 in the two branches is the same, the medium relaxes with different velocities. Starting from the
 14 elastic solution proposed by Okada [1992] for a tabular dislocation source embedded in an elastic
 15 and homogeneous half-space, Piombo et al. [2007] applied the "Correspondence Principle" of linear
 16 viscoelasticity which states that the Laplace transform of the solution to any deformation problem
 17 with a linear rheology can be expressed in the form of the corresponding elastic solution, given a
 18 suitable choice of Laplace-transformed effective shear modulus. In this way, the authors derived the
 19 quasi-static displacement, strain and stress fields for finite rectangular dislocations in a viscoelastic,
 20 homogeneous and isotropic half-space, assuming a viscoelastic deformation with respect to both the
 21 shear and the normal stresses (keeping a constant bulk modulus) and with a shear modulus relaxing
 22 as Maxwell fluid. The relaxation times derived by Piombo et al. [2007] for faults embedded in a
 23 viscoelastic halfspace are:

$$\begin{aligned}
 \tau_1 &\equiv 3 \frac{\lambda + \mu}{3\lambda + 2\mu} \tau_0 \\
 \tau_2 &\equiv 3 \frac{\lambda + 2\mu}{3\lambda + 2\mu} \tau_0
 \end{aligned}
 \tag{1}$$

1 where $\tau_0 = \frac{\eta}{G_0\mu}$ is the Maxwell relaxation time and characterizes the rate of decay of stress, while
2 λ and μ are the first Lamè constant and the shear modulus, respectively and η is the viscosity. The
3 relaxation times are related to the use of two spring-dashpot elements. The use of the relaxation
4 times calculated for a tabular dislocation source [Piombo et al., 2007] is appropriate because it is the
5 same type of dislocation that we used in this work for simulate the dike-forming intrusions [Aloisi
6 et al., 2011], Figure 2. In our case, however, we are one step further because we consider a
7 heterogeneous 3D domain where the physical properties change both with depth and horizontally
8 based on realistic tomographic results as shown in Aloisi et al. [2002]. Therefore, Lamè constants
9 change inside our domain, and, in the same way, the relaxation times. In other terms, each zone
10 relaxes with respect to its “local” relaxation time. This is a great advantage with respect to previous
11 studies, because the relaxation times are not the same for all the studied area but depend on the
12 considered physical properties deduced by the seismic tomography. According to the
13 “Correspondence Principle”, the bulk modulus is kept constant while the medium deforms in a
14 viscoelastic manner with respect to both the shear and the normal stresses. In our model, there is no
15 violation of this Principle, since the bulk modulus (as the other constants) is still locally constant.
16 This means that the bulk modulus is constant under the substitution of the new “local” Lamè
17 constants obtained by the Laplace transform, but only for the values that these constants assume in
18 specific zones of the domain.

19 Below 6 km depth (Fig. 2), we included a plastic layer representing the ductile carbonates
20 substrate corresponding to the Hyblean Plateau that starts at about a depth of 5 km underneath the
21 volcanic edifice and has an average thickness of about 10 km. As said before, Heap et al. [2013]
22 and Bakker et al. [2015] have in fact demonstrated that thermal-stressing induces a progressive and
23 significant change in the physical properties of the Etnean carbonate basement and that, above 500°,
24 the rocks deform in a ductile manner. They speculate that this ductile behaviour could be a key
25 factor in explaining volcano instability. In our model, the plastic behaviour is set in the form of a

1 perfectly plastic material with a yield strength of 300 MPa, which is consistent with experimental
2 values as described in Heap et al. [2013] and Bakker et al. [2015].

3 No gravitational load is applied because, as demonstrated in Aloisi et al. [2011], its contribution
4 is small with respect to the total displacement and can then be avoided. The other model settings
5 (geometry, mesh and boundary conditions) are referred to Aloisi et al. [2011], Figure 1.

6 The aim of our viscoelastic/plastic FEM model is to investigate the temporal link between the
7 push of the 2002-2003 dike-forming intrusions and the movements on the principal fault systems, in
8 relation to the recorded seismicity. In particular, we investigated if the stress change due to the
9 magma intrusion in the S and NE Rift was responsible for the 27 October 2002 Pernicana
10 earthquake (01.28 GMT; $M_d = 3.5$) and for the 29 October 2002 Timpe fault system earthquake
11 (10.02 GMT; $M_d = 4.4$). The path of the magmatic intrusions can be estimated by seismic activity
12 [Barberi et al., 2004; Aloisi et al., 2006]. In particular, Barberi et al. [2004] analyzed the spatio-
13 temporal evolution of the epicentral pattern during the period 26-29 October 2002 and Aloisi et al.
14 [2006] analytically modelled the composite intrusion of the two dikes, using seismic and tilt data.
15 These analyses show that, from 21.00 GMT to 23.30 GMT on 26 October, a near vertical tensile
16 dike-forming intrusion propagated on the southern upper flank. Successively, the recorded data
17 show that, from 00.10 GMT on 27 October, a complex dike-forming intrusion propagated laterally
18 along the NE Rift, reaching the western tip of the Pernicana Fault at about 23.00 GMT, 27 October.
19 The intrusion has also been documented by the formation of a series of eruptive fissures and
20 explosive activity in correspondence of the dike path [Spampinato et al., 2008]. During the dike-
21 forming intrusions, the first, here studied, earthquake (27 October 2002, 01.28 GMT, $M_d = 3.5$) was
22 recorded. After about thirty-five hours from the starting of the interaction between the NE dike-
23 forming intrusion and the Pernicana Fault, also evidenced by compressive focal mechanism
24 [Barberi et al., 2004; Aloisi et al., 2006], the second, here studied, earthquake (29 October 2002,
25 10.02 GMT, $M_d 4.4$) was generated.

1 Therefore, following the results in time and dislocations obtained from the above, we
2 reproduced the magmatic intrusions by activating the dikes sequentially (Fig. 2). First we activated
3 the south dike (extending from 0.5 km b.s.l. to the volcano surface and having a length of 1.6 km)
4 prescribing an opening component of 0.5 m and, then, the north-east dike, which is modelled in two
5 distinct pieces: a first part (extending from 2.0 km b.s.l. to the volcano surface and having a length
6 of 2.5 km), which has an opening component of 1.7 m and a second part (extending from 2.0 km
7 b.s.l. to the volcano surface and having a length of 3.5 km), which has an opening component of 0.3
8 m and a left strike slip component of 1 m (Aloisi et al., 2011). All the components of these three
9 dikes are gradually activated in time from zero to each maximum value through a linear function. In
10 particular, the south dike is activated from the beginning of the simulation (21.00 GMT on 26
11 October) to 2.5 hours after (23.30 GMT on 26 October), and then its maximum opening value is
12 kept constant (to avoid a linear backward response). Successively, the first north east dike is
13 gradually activated from 00.10 GMT to 02.00 GMT, on 27 October. Finally, while the south dike
14 and the first north eastern dike opening components are kept at their maximum values, the second
15 part of the north eastern dike is gradually activated from the 02.00 GMT to the 16.00 GMT, on 27
16 October (Aloisi et al., 2006). All the three magmatic intrusions keep the maximum values of their
17 dislocation components until the end of the simulation, which is set at a total time of 65 hours,
18 across the time of occurrence of the M_d 4.4 earthquake, along Santa Venerina Fault (29 October
19 2002, 10:02 GMT).

20 To see if Pernicana and Santa Venerina earthquakes were generated by the intrusions, we
21 monitored the variation of the CSC during the time, considering the intrusions as the sources of the
22 stress change, and looking at the CSC on a left lateral, about E-W, strike-slip fault (western part of
23 Pernicana Fault) and on a right lateral, about NW-SE, strike-slip fault (Timpe fault system). To do
24 this, our time-dependent model is set as following: in the first phase (co-intrusive period), the
25 southern and north-eastern dikes intrude, through the time, as described above and the chosen time
26 step for this phase is half an hour. In the second phase (post-intrusive period), the simulation goes

1 further through the time, until the 29 October, with a time step of 1 hour. These time steps have
2 been chosen after different tests, in order to balance between the computational time and an
3 accurate description of the phenomena.

4 During the first phase, we verified if the CSC on the Pernicana Fault is big enough to trigger the
5 01.28 GMT, $M_d = 3.5$, earthquake. In the second phase, we analysed instead the evolution of the
6 CSC considering two different cases. In the first case, the magma intrusions are considered as the
7 only responsible of the CSC evolution in the area of Santa Venerina Fault. For this case, we
8 computed the CSC values to see if they were big enough to trigger the Santa Venerina earthquake.
9 In the second case instead, we evaluated the combined contribution of the magma intrusions
10 together with the Pernicana earthquake on the Santa Venerina seismicity. In this case, Pernicana
11 fault was activated from the time of the $M_d 3.5$ earthquake for 30 minutes, that is the simulation
12 time step, applying a left lateral strike slip component of 0.7 m [Neri et al., 2004], considering the
13 effect of the pre-stress state for acting intrusive dynamics, cumulated during the interseismic period
14 [Neri et al., 2004; Bonforte et al., 2007b; Puglisi et al., 2008; Currenti et al., 2012; Alparone et al.,
15 2013a and 2013b; Ruch et al., 2013]. In this way, we kept into account the overall dislocation, along
16 of the Pernicana Fault, produced by the Pernicana earthquake and by the push of the magmatic
17 intrusions. The aim of this investigation is to see if the Santa Venerina earthquake may have been
18 triggered by the Pernicana stress transfer in a chain process, which starts from the South and North-
19 East magma intrusions first. Results of these investigations are showed in the following section.

20

21 **4. Results and discussions**

22

23 Figure 3 shows the temporal evolution of the CSC on Pernicana fault plane at the hypocentral
24 location of the 27th October, 01.28 GMT earthquake (1.6 km, a.s.l.). Three hours after the start of
25 the magma intrusion (00.00 GMT on 27 October), the CSC values are still not enough (0.03 bar) to
26 justify an activation of the fault. As discussed before, the range of stress for triggering an

1 earthquake depends in fact on many factors related to the area of study but it has been shown that,
2 in average, an increment of about 0.1 bar, with respect to the initial stress state, can be enough to
3 trigger an earthquake [Stein, 1999; Bonanno et al., 2011; Privitera et al., 2012; Gonzalez and
4 Palano, 2014]. Therefore, at the 00.00 GMT on 27 October, we are surely under this approximate
5 minimum level and consequently, according to our simulations, the southern intrusion was not
6 responsible for the Pernicana earthquake. Three and half hours after the intrusion (00.30 GMT on
7 27 October, Fig. 3), the CSC reaches a value of about +1.3 bar, surely big enough to trigger
8 Pernicana earthquake that would take place an hour later, when the CSC reaches a value of about
9 +1.5 bar (Fig. 3). Therefore, we found that the first part of the north-east dike intrusion was able to
10 activate Pernicana fault, about when the maximum value of the CSC is reached and consequently
11 our model was able to predict accurately enough the time of the Pernicana earthquake. When the
12 second part of the north-east dike intrudes, the CSC starts to decrease, tending to discourage left-
13 lateral strike slip dislocations. In particular, using the classification of Kaverina et al. [1996] and
14 Kagan [2005], four of the focal mechanisms, recorded few hours after the left-lateral strike slip, M_d
15 3.5, earthquake, when the CSC becomes negative, show strike-slip together with thrust
16 characteristics (Fig. 3). This behaviour can be interpreted as the effect of the final interaction of the
17 intrusion with the western tip of Pernicana fault, where it slowed and stopped. Also Currenti et al.
18 [2008a] found that the stress change area surrounding Pernicana Fault well matches the seismicity
19 recorded from 27 to 29 October. The boundary elements models, developed by Walter et al. [2005],
20 show a significant increase of the Coulomb failure stress at the western end of the Pernicana Fault.
21 The two models previously mentioned, however, do not consider any dynamic effect as they run
22 stationary. Our model instead is timely dependent and, therefore, for the first time, allowed as to
23 described in detail how the CSC changes evolved in time, increasing and decreasing in response to
24 the emplacement of various dike-forming intrusions. Our model, taking into account the principal
25 fault systems with specified friction coefficients, can explain clearly how tectonic faults respond in
26 different manner to the position of magmatic intrusions. Moreover, it allows looking at the CSC

1 directly on the fault plane (Fig. 4). Results show that positive CSC are lower, with respect to the
2 other parts of the fault plane, about at the sea level. Higher CSC values appear in two small areas
3 above and under the sea level. The area included between the free surface and the sea level is in
4 accordance with the estimated hypocentral location (Fig. 4) and is more circumscribed than the
5 results provided by Walter et al [2005].

6 Aloisi et al. [2003] found that the north-eastern intrusion was the primary cause of the recorded
7 deformation pattern, while the southern dike gave only a minimal contribution. Our results clearly
8 demonstrated that exactly the NE intrusion is compatible with the reactivation of the Pernicana
9 fault, and, in particular, exclusively the first part of the intrusion. As found by other authors (e.g.,
10 Ferlito et al., 2009) this is consistent with the kinematic of the NE Rift, which plays a very active
11 role in the activity of Mt. Etna volcano, for its extensional tectonics, that allows the intrusion and
12 residence of magma bodies at various depths, and for the interaction it has with seismogenetic
13 structures [Neri et al., 2004; Bonforte et al., 2007b; Puglisi et al., 2008; Currenti et al., 2012;
14 Alparone et al., 2013a and 2013b; Ruch et al., 2013].

15 Figure 5 shows the temporal evolution of the CSC on the Santa Venerina fault plane at the
16 depth of the 29th October, 10.00 GMT earthquake (0.7 km, b.s.l.). After six hours from the start of
17 the magma intrusions, the CSC for Santa Venerina fault, as induced by dike-forming intrusions
18 exclusively, reached a value of about +0.1 [bar], (line with white diamonds in Figure 5). This result
19 allows us to infer that, probably, Santa Venerina earthquake could have been triggered by magma
20 intrusions, only. But, as said before, an increment of about 0.1 bar, with respect to the initial stress
21 state, can be seen as an almost lower limit value to trigger an earthquake. Therefore, we decided to
22 verify if there are other active processes that, combined with the dike-induced stresses, can be better
23 explain the Santa Venerina earthquake. Similarly, Currenti et al. [2008a] looked at the static stress
24 changes onto the Timpe fault system and obtained a low value of CSC, compatible with our results.
25 Walter et al. [2005] found instead a negative value, still suggesting that the faulting on the Santa

1 Venerina Fault is discouraged by the dike intrusions. They speculated that this fault was coupled to
2 movement of the Pernicana fault and not so much to shallow level intrusions.

3 Therefore, might the earthquake on Santa Venerina fault have been triggered by Pernicana fault,
4 in combination with the dike-forming intrusion? This question is plausible if we consider the slip
5 observed on Pernicana Fault, unlocked by the 2002-2003 magmatic intrusion, as the result of the
6 stress accumulated during inter-seismic periods by response to previous intrusive dynamics, acting
7 on the high eastern and northeastern portion of the volcano. According to this point of view, the slip
8 observed on Pernicana Fault would have two components, (a) the push of the dike-intrusions and
9 (b) the movement related to the stress previously accumulated and then suddenly released, during
10 the M_d 3.5 earthquake. Consequently, Pernicana Fault (that, until now, has been treated as a passive
11 receiving crustal discontinuity) has to be activated, exclusively in the western segment, by choosing
12 the value of slip that this segment had during the first day of eruption, according to field campaign
13 measurements (about 0.7 m of strike slip component; Neri et al., 2004). When Pernicana Fault is
14 activated, the CSC value on Santa Venerina Fault rises up to about +0.4 bar in circa 20 hours, (line
15 with gray diamonds in Figure 5), which is higher with respect to the 0.1 bar, value acceptable for
16 encouraging the fault movement. Also Walter et al. [2005] proposed that Pernicana left-lateral
17 faulting encouraged the movement along Santa Venerina Fault, pointing out to the importance of
18 the fault-fault interaction (see also Neri et al., 2004). However, differently from Walter et al. [2005]
19 that imposed a left-lateral displacement along the entire Pernicana Fault, we obtained that the
20 faulting of the western segment only could have been already enough to encourage the start of the
21 seismic swarms at the Timpe fault system. In fact, if we observe the CSC (Fig. 6), at the time of the
22 Santa Venerina earthquake, on an horizontal plane cutting the domain at the hypocentral depth (0.7
23 km b.s.l.), the positive lobe “L” in the area of the earthquake is much more wide when Pernicana
24 fault is activated (Fig. 6a2) with respect to the case when only the effects of the magmatic intrusions
25 are considered (Fig. 6a1). In particular, the lobe “L” extends much further southwards and
26 eastwards, reaching the Timpe fault systems (Fig. 6a2). The comparison between the two cases

1 above is also clear at depth (Fig. 6b1 and Fig. 6b2). Cutting the domain vertically along an about
2 NW-SE slice (profile AA') passing through the Santa Venerina fault, we obtained a clearly positive
3 CSC zone, corresponding with the hypocentral depth when Pernicana fault is activated ("L" in Fig.
4 6b2).

5 Alparone et al. [2013b] revealed a significant temporal correlation between periods of large
6 deformation of the eastern flank and intensified seismic activity along the northern border
7 (Pernicana fault system). For example, the seismicity along Pernicana fault system, recorded in the
8 1984, was followed by an increased deformation rate of the eastern flank that continued until 1987.
9 Between 1987 and 2001, the seismicity and the deformations were both reduced. Azzaro et al.
10 [2013] confirmed that the local seismicity is closely related to the flank dynamics and, in particular,
11 they underlined the important role of the Timpe fault system in the seismic hazard affecting the
12 eastern flank. Therefore, the common temporal evolution of the Pernicana kinematics and of the
13 eastern flank activity demonstrates that there is a clear correlation between the two processes, as we
14 also obtained.

15 Regarding the temporal evolution of the CSC on Santa Venerina fault (Fig. 5), our model is not
16 able to predict exactly the time of the M_d 4.4 earthquake because the maximum CSC value is
17 reached several hours before, about at the end of the north-east intrusion time and this value
18 remains more or less constant during the time. However, during this time interval, some
19 earthquakes were recorded in the area around the M_d 4.4 earthquake, showing a kinematic
20 compatible with the estimated CSC (Fig. 5). Moreover, across the end of our simulation, other two
21 strong earthquakes were recorded in the South East sector (29 October 16.39 GMT, $M_d = 4.0$ and
22 17.14 GMT, $M_d = 4.1$) showing focal mechanisms compatible with the Santa Venerina M_d 4.4
23 earthquake [Monaco et al., 2005] and, therefore, well explained by our model.

24 Finally, is noteworthy to say that the presence of the ductile substrate (carbonates) does not
25 appear to be affected, in term of stress, by the dike intrusions. In particular, the maximum stress
26 induced in the ductile layer by the intruding dikes is about 1 MPa, which is one order of magnitude

1 lower than the minimum yield stress (10 MPa) for such rocks at this depth and under thermal
2 weakening condition [Heap et al., 2013; Bakker et al., 2015].

3

4 **5. Conclusions**

5

6 A 3D highly realistic FEM numerical model has been carried out to investigate the temporal
7 evolution of CSC caused by dyke-forming intrusions during the 2002-2003, Mt. Etna eruption, in a
8 viscoelastic/plastic rheology. The model allowed us to describe in detail how the CSC evolved in
9 time, increasing and decreasing in response to the emplacement of various dike-forming intrusions.
10 Therefore, our model can explain better how etnean faults respond in different manner to the
11 position of magmatic intrusions. It has been showed that the dike-forming intrusions are responsible
12 for the activation of Pernicana fault accordingly to the time and position of the 27th October 2002,
13 01:28 GMT earthquake ($M_d = 3.5$). Moreover, the earthquake on Pernicana fault, combined with the
14 dike-induced stresses, may have triggered the earthquake on Santa Venerina fault (29 October 10:02
15 GMT, $M_d = 4.4$). Our results confirm the significant interplay between the processes observed in
16 the eastern flank and underline the key role of the NE Rift in the activity of Mt. Etna volcano.
17 Therefore, the knowledge of stress change rates is a powerful tool for assessing seismic hazards, as
18 it cannot only be used to understand past events, but also to predict where future earthquakes are
19 likely to occur.

20

21 **Acknowledgments**

22 This work was supported by MED-SUV Project. We thank Danila Scandura for the debate
23 about governing equations for ground deformation. We thank Antonio Scaltrito and Graziella
24 Barberi (INGV, Osservatorio Etneo, Catania) for the fruitful discussion on the 2002-2003 etnean
25 seismicity. We thank Luciano Scarfî for the discussion about the estimated focal mechanisms. We

1 thank Salvo Gambino for the tips about the explanation of the results. Finally, we thank Mimmo
2 Palano and Flavio Cannavò for the general tips.

3

4 **Captions**

5 Figure 1 - Map of Mount Etna. A sketch map of the fault systems is reported, together with the most
6 active crustal discontinuities modelled in the paper (heavy black lines) and the NE and south rift
7 zones. The 2002–2003 erupted lava flows and the principal vents are indicated. Moreover, the
8 surface projection of the modelled 2002–2003 dike - forming intrusions is shown (solid gray lines
9 in the lower inset), together with the magma pathways historically resolved by GPS, seismic, and
10 other geophysical data. In the upper inset, the location of Mount Etna in the central Mediterranean
11 area is shown, at the footwall of the Malta Escarpment. Moreover, in the upper inset, the meshed
12 domain is reported. The mesh elements were gradually refined from the domain bottom to the fault
13 systems and the ground surface. Epicentral location and focal mechanisms of the two studied
14 earthquakes are also shown. Redrawn from Aloisi et al. [2011].

15 Figure 2 - Time-dependent model with the dimensions of each layer of the introduced rheology. The
16 dike-forming intrusions with the respective dislocation components are showed. Young's modulus
17 deduced by the seismic tomography of Aloisi et al. [2002] is also reported along the cross-section.
18 Redrawn from Aloisi et al. [2006].

19 Figure 3 - Temporal evolution of the Coulomb stress changes resolved at the hypocentral location
20 of the 27th October, 01.28 GMT earthquake (1.6 km, a.s.l.). The earthquakes (little squares)
21 recorded in a range of 2 km around the 27th October earthquake, together with the available
22 corresponding focal mechanisms [Barberi et al., 2004], are also reported.

23 Figure 4 - Coulomb stress changes resolved on Pernicana fault plane at the 01.00 GMT and 01.30
24 GMT on 27 October, about the time of Pernicana M_d 3.5 earthquake. The white square indicates the
25 hypocentral location of the 27th October, 01.28 GMT earthquake.

1 Figure 5 - Temporal evolution of the Coulomb stress changes resolved at the hypocentral location
2 of the 29th October, 10.02 GMT earthquake (0.7 km, b.s.l.). The line with white diamonds reports
3 the CSC as induced by dike-forming intrusions exclusively (Pernicana passive). Whereas, the line
4 with gray diamonds reports the CSC when Pernicana fault is activated. The earthquakes (little
5 squares) recorded in a range of 2 km around the 29th October earthquake, together with the available
6 corresponding focal mechanisms [Barberi et al., 2004; Monaco et al., 2005], are also reported.

7 Figure 6 - Coulomb stress changes resolved, at the time of Santa Venerina earthquake (10.02 GMT
8 on the 29th October), along a mapview at 0.7 km b.s.l. (hypocentral depth), in the case Pernicana
9 passive (a1) and active (a2) and along a cross-section passing through the profile AA', in the case
10 Pernicana passive (b1) and active (b2). The white square indicates the location of the 29th October
11 earthquake. The letter "L" indicates the positive lobe extending much further southwards and
12 eastwards when Pernicana fault is activated (see text for details).

13

14 **References**

15 Acocella, V., Behncke B., Neri M., DAmico S., 2003. Link between major flank slip and 2002-
16 2003 eruption at Mt. Etna (Italy). *Geophysical Research Letters*, 30, 24, 2286.
17 doi:10.1029/2003GL018642.

18 Aloisi, M., Cocina, O., Neri, G., Orecchio, B., Privitera, E., 2002. Seismic tomography of the
19 crust underneath the Etna volcano, Sicily, *Phys. Earth Planet. Inter.*, 134, 139–155,
20 doi:10.1016/S0031-9201(02) 00153-X.

21 Aloisi, M., Bonaccorso, A., Gambino, S., Mattia, M., Puglisi, G., 2003. Etna 2002 eruption
22 imaged from continuous tilt and GPS data. *Geophysical Research Letters*, 30, 23, 2214. doi:
23 10.1029/2003GL018896.

24 Aloisi, M., Bonaccorso, A., Gambino, S., 2006. Imaging composite dike propagation (Etna,
25 2002 case), *J. Geophys. Res.*, 111, B06404, doi:10.1029/2005JB003908.

1 Aloisi, M., Bonaccorso, A., Cannavò, F., Gambino, S., Mattia, M., Puglisi, G., Boschi, E. 2009.
2 A new dike intrusion style for the Mount Etna May 2008 eruption modelled through continuous tilt
3 and GPS data, *Terra Nova*, 21, 316–321, doi:10.1111/j.1365-3121.2009.00889.x.

4 Aloisi, M., Mattia, M., Monaco, C., Pulvirenti, F., 2011. Magma, faults, and gravitational
5 loading at Mount Etna: The 2002–2003 eruptive period. *J. Geophys. Res.*, 116, B05203.
6 doi:10.1029/2010JB007909.

7 Alparone, S., Cocina, O., Gambino, S., Mostaccio, A., Spampinato, S., Tuvè, T., Ursino, A.,
8 2013a. Seismological features of the Pernicana–Provenzana Fault System (Mt. Etna, Italy) and
9 implications for the dynamics of northeastern flank of the volcano. *Journal of Volcanology and*
10 *Geothermal Research*, 251, 16-26. doi:10.1016/j.jvolgeores.2012.03.010.

11 Alparone, S., A. Bonaccorso, A. Bonforte, Currenti, G., 2013b. Long-term stress-strain analysis
12 of volcano flank instability: The eastern sector of Etna from 1980 to 2012, *J. Geophys. Res. Solid*
13 *Earth*, 118, 5098–5108, doi:10.1002/jgrb.50364.

14 Alparone, S., Maiolino, V., Mostaccio, A., Scaltrito, A., Ursino, A., Barberi, G., D’Amico, S.,
15 Di Grazi, a G., Giampiccolo, E., Musumeci, C., Scarfì, L., Zuccarello, L., 2015. Instrumental
16 seismic catalogue of Mt. Etna earthquakes (Sicily, Italy): ten years (2000-2010) of instrumental
17 recordings. *Annals of Geophysics*, 58, 4, 2015, S0435; doi:10.4401/ag-6591.

18 Anderson, G., Johnson, H., 1999. A new statistical test for static stress triggering: Application to
19 the 1987 Superstition Hills earthquake sequence. *J. Geophys. Res.* 104, 20153-20168. doi:
20 10.1029/1999JB900200.

21 Andronico, D., Branca, S., Calvari, S., Burton, M., Caltabiano, T., Corsaro, R. A., Del Carlo, P.,
22 Garfì, G., Lodato, L., Miraglia, L., Murè, F., Neri, M., Pecora, E., Pompilio, M., Salerno, S.,
23 Spampinato, L., 2005. A multi-disciplinary study of the 2002-03 Etna eruption: Insights into a
24 complex plumbing system, *Bull. Volcanol.*, 67, 314–330, doi:10.1007/s00445-004-0372-8.

1 Andronico, D., Scollo, S., Caruso, S., Cristaldi, A., 2008. The 2002-03 Etna explosive activity:
2 Tephra dispersal and features of the deposits, *J. Geophys. Res.*, 113, B04209.
3 doi:10.1029/2007JB005126.

4 Azzaro, R., D'Amico, S., Peruzza, L., Tuvè, T., 2013. Probabilistic seismic hazard at Mt. Etna
5 (Italy): The contribution of local fault activity in mid-term assessment. *Journal of Volcanology and*
6 *Geothermal Research*, 251, 158–169. doi:10.1016/j.jvolgeores.2012.06.005.

7 Bakker, R.R., Violaya, M.E.S., Benson, P.M., Vinciguerra, S.C., 2015. Ductile flow in sub-
8 volcanic carbonate basement as the main control for edifice stability: New experimental insights.
9 *Earth and Planetary Science Letters*, 430, 533–541, <http://dx.doi.org/10.1016/j.epsl.2015.08.017>.

10 Barberi, G., Cocina, O., Neri, G., Privitera, E., Spampinato, S., 2000. Volcanological inferences
11 from seismic strain tensor computations at Mt. Etna Volcano, Sicily, *Bull. Volcanol.*, 62, 318 – 330.

12 Barberi, G., Cocina, O., Maiolino, V., Musumeci, C., Privitera, E., 2004. Insight into Mt. Etna
13 (Italy) kinematics during the 2002-2003 eruption as inferred from seismic stress and strain tensors.
14 *Geophys. Res. Lett.*, 31, L21614. doi:10.1029/2004GL020918.

15 Bonaccorso, A., Aloisi, M., Mattia, M., 2002. Dike emplacement forerunning the Etna July
16 2001 eruption modeled through continuous tilt and GPS data, *Geophys. Res. Lett.*, 29(13), 1624,
17 doi:10.1029/2001GL014397.

18 Bonanno, A., Palano, M., Privitera, E., Gresta, S., Puglisi, G., 2011. Magma intrusion
19 mechanisms and redistribution of seismogenic stress at Mt. Etna volcano (1997-1998). *Terra Nova*,
20 23, 339-348, doi:10.1111/j.1365-3121.2011.01019.x, 2011.

21 Bonforte, A., Gambino, S., Guglielmino, F., Obrizzo, F., Palano, M., Puglisi, G., 2007a. Ground
22 deformation modeling of flank dynamics prior to the 2002 eruption of Mt. Etna. *Bull. Volcanol.*, 69,
23 757-768. doi: 10.1007/s00445-006-0106-1.

24 Bonforte, A., Carbone, D., Greco, F., Palano, M., 2007b. Intrusive mechanism of the 2002 NE-
25 rift eruption at Mt Etna (Italy) modelled using GPS and gravity data. *Geophys. J. Int.*, 169, 339–
26 347. doi: 10.1111/j.1365-246X.2006.03249.x.

1 Branca, S., Ferrara, V., 2001. An example of river pattern evolution produced during the lateral
2 growth of a central polygenic volcano: the case of the Alcantara river system, Mt Etna (Italy).
3 *Catena*, 45/2, 85-102. doi:10.1016/S0341-8162(01)00144-8.

4 Briole, P., Massonnet, D., Delacourt, C., 1997. Post-eruptive deformation associated with the
5 1986–87 and 1989 lava flows of Etna detected by radar interferometry. *Geophys. Res. Lett.* 24, 37–
6 40. doi: 10.1029/96GL03705.

7 Bruno, V., Mattia, M., Aloisi, M., Palano, M., Cannavò, F., Holt, W.E., 2012. Ground
8 deformations and volcanic processes as imaged by CGPS data at Mt. Etna (Italy) between 2003 and
9 2008. *Journal of Geophysical Research – Solid Earth*, 117, B07208, doi:10.1029/2011JB009114.

10 Cai, J. G., 2001. Effects of Parallel Fractures on wave attenuation in rock. School of Civil and
11 Structural Engineering, PhD thesis. Nanyang Technological University, Singapore, p 306.

12 Calais, E., Freed, A., Mattioli, G., Amelung, F., Jónsson, S., Jansma, P., Hong, S.H., Dixon, T.,
13 Prepetit, C., Momplaisir, R., 2010. The January 12, 2010, Mw 7.0 earthquake in Haiti: context and
14 mechanism from an integrated geodetic study, *Nature Geosciences*, doi 10.1038/NNGEO992.

15 Cannavó, F., Arena, A., Monaco, C., 2014. Local geodetic and seismic energy balance for
16 shallow earthquake prediction. *Journal of Seismology*, 1-8. doi: 10.1007/s10950-014-9446-z.

17 Chiarabba, C., Amato, A., Boschi, E., Barberi, E., 2000. Recent seismicity and tomographic
18 modeling of the Mount Etna plumbing system. *Journal of Geophysical Research* 105, 10923–10938.
19 doi: 10.1029/1999JB900427.

20 Chiocci, F.L., Coltelli, M., Bosman, A., Cavallaro D. 2011. Continental margin large-scale
21 instability controlling the flank sliding of Etna volcano. *Earth and Planetary Science Letters*,
22 Volume 305, Issues 1-2, 1 May 2011, Pages 57-64. doi: 10.1016/j.epsl.2011.02.040.

23 Cocina, O., Neri, G., Privitera, E., Spampinato, S., 1997. Stress tensor computations in the
24 Mount Etna area (southern Italy) and tectonic implications, *J. Geodyn.*, 23, 109–127,
25 doi:10.1016/S0264-3707(96)00027-0.

1 Corsaro, R. A., Pompilio, M., 2004. Buoyancy-controlled eruption of magmas at Mt Etna, Terra
2 Nova, 16, 16–22, doi:10.1046/j.1365-3121.2003.00520.x.

3 Currenti, G., Del Negro, C., Johnston, V., Sasai Y., 2007. Close temporal correspondence
4 between geomagnetic anomalies and earthquakes during the 2002–2003 eruption of Etna volcano, J.
5 Geophys. Res., 112, B09103. doi:10.1029/2007JB005029.

6 Currenti, G., Del Negro, C., Ganci, G., Williams, C.A., 2008a. Static stress changes induced by
7 the magmatic intrusions during the 2002-2003 Etna eruption. J. Geophys. Res. 113, B10206.
8 doi:10.1029/2007JB005301.

9 Currenti, G., Piombo, A., Del Negro, C., Dragoni, M., 2008b. Piezomagnetic fields due to an
10 inclined rectangular fault in a viscoelastic half-space: an application to the 2002–2003 Etna
11 eruption. Geophysical Journal International, 175, 3, 901–912. doi: 10.1111/j.1365-
12 246X.2008.03941.x.

13 Currenti, G., Bonaccorso, A., Del Negro, C., Guglielmino, F., Scandura, D., Boschi, E., 2010.
14 FEM-based inversion for heterogeneous fault mechanisms: application at Etna volcano by DInSAR
15 data. Geophysical Journal International, 183, 2, 765-773. doi: 10.1111/j.1365-246X.2010.04769.x.

16 Currenti, G., Solaro, G., Napoli, R., Pepe, A., Bonaccorso, A., Del Negro, C., Sansosti, E.,
17 2012. Modeling of ALOS and COSMO-SkyMed satellite data at Mt Etna: Implications on relation
18 between seismic activation of the Pernicana fault system and volcanic unrest. Remote Sensing of
19 Environment, 125, 64–72. <http://dx.doi.org/10.1016/j.rse.2012.07.008>.

20 De Gori, P., Chiarabba, C., Giampiccolo, E., Martinez-Arèvalo, C., Patanè, D., 2011. Body
21 wave attenuation heralds incoming eruptions at Mount Etna. Geology, 39, 503-506. doi:
22 10.1130/G31993.1.

23 Del Negro, C., Currenti, G., Napoli, R., Vicari, A., 2004. Volcanomagnetic changes
24 accompanying the onset of the 2002–2003 eruption of Mt. Etna (Italy). Earth and Planetary Science
25 Letters, 229, 1-14. doi:10.1016/j.epsl.2004.10.033.

1 Del Negro, C., Currenti, G., Scandura, D., 2009. Temperature-dependent viscoelastic modeling
2 of ground deformation: Application to Etna volcano during the 1993–1997 inflation period. *Physics*
3 *of the Earth and Planetary Interiors*, 172, 3–4, 299–309. doi: 10.1016/j.pepi.2008.10.019.

4 De Lorenzo, S., Giampiccolo, E., Martinez-Arevalo, C., Patanè, D., Romeo, A., 2010. Fault
5 plane orientations of microearthquakes at Mt. Etna from the inversion of P-wave rise times. *Journal*
6 *of Volcanology and Geothermal Research*, 189, 247–256. doi:10.1016/j.jvolgeores.2009.11.011.

7 Dragonì, M., Bonafede, M., Boschi, E., 1982. Stress relaxation in the Earth and seismic activity,
8 *Rivista del Nuovo Cimento*, 5, 2, 1–34. doi: 10.1007/BF02740828.

9 Ellis, M., King, G. 1991. Structural control of flank volcanism in continental rifts, *Science*, 254,
10 839–842, doi:10.1126/science.254.5033.839.

11 Ferlito C., Coltorti M., Cristofolini P., Giacomoni P.P., 2009. The contemporaneous emission of
12 low-K and high-K trachybasalts and the role of the NE Rift during the 2002 eruptive event, Mt.
13 Etna, Italy. *Bulletin of Volcanology*, 71, 5, 575–587. doi: 10.1007/s00445-008-0243-9.

14 Feuillet, N., Cocco, M., Musumeci, C., Nostro, C., 2006. Stress interaction between seismic
15 and volcanic activity at Mt. Etna. *Geophys. J. Int.*, 164, 697–718. doi:10.1111/j.1365-
16 246X.2005.02824.x.

17 Freed, A. M., Lin, J., 1998. Time-dependent changes in failure stress following thrust
18 earthquakes. *J. Geophys. Res.* 103, 24393±24410 (1998). doi: 10.1029/98JB01764.

19 Freed, A.M., Lin, J., 2001. Delayed triggering of the 1999 Hector Mine earthquake by
20 viscoelastic stress transfer, *Nature*, 411, 180–183. doi:10.1038/35075548.

21 Gambino, S., Mostaccio, A., Patanè, D., Scarfi, L., Ursino, A., 2004. High-precision locations
22 of the microseismicity preceding the 2002–2003 Mt. Etna eruption. *Geophysical Research Letters*,
23 31, L18604. doi:10.1029/2004GL020499.

24 Gonzalez, P. J., Palano, M., 2014. Mt. Etna 2001 eruption: New insights into the magmatic
25 feeding system and the mechanical response of the western flank from a detailed geodetic dataset.

1 Journal of Volcanology and Geothermal Research, 274, 108–121.
2 <http://dx.doi.org/10.1016/j.jvolgeores.2014.02.001>.

3 Gross, S., Kisslinger, C., 1997. Estimating tectonic stress rate and state with Landers
4 aftershocks. *J. Geophys. Res.* 102, 7603-7612. doi: 10.1029/96JB03741.

5 Gruppo Analisi Dati Sismici, 2014. Catalogo dei terremoti della Sicilia Orientale - Calabria
6 Meridionale (1999-2014). INGV, Catania, <http://www.ct.ingv.it/ufs/analisti/catalogolist.php>.

7 Harris, R. A., Simpson, R. W., 1992. Changes in static stress on southern California faults after
8 the 1992 Landers earthquake. *Nature* 360, 251-254. doi:10.1038/360251a0.

9 Harris R.A., 1998. Introduction to Special Section: Stress Triggers, Stress Shadows, and
10 Implications for Seismic Hazard. *Journal of Geophysical Research*, 103, B10, 24,347-24,358. doi:
11 10.1029/98JB01576.

12 Heap, M.J., Mollo, S., Vinciguerra, S., Lavallée, Y., Hess, K.U., Dingwell, D.B., Baud, P.,
13 Iezzi, G., 2013. Thermal weakening of the carbonate basement under Mt. Etna volcano (Italy):
14 Implications for volcano instability. *Journal of Volcanology and Geothermal Research*, 250, 42–60.
15 <http://dx.doi.org/10.1016/j.jvolgeores.2012.10.004>.

16 Hearn, E.H., Bürgmann, R., Reilinger, R., 2002. Dynamics of Izmit earthquake postseismic
17 deformation and loading of the Düzce earthquake hypocenter. *Bull. Seismol. Soc. Am.* 92, 172–
18 193. doi: 10.1785/0120000832.

19 Hearn, E.H., 2003. What can GPS data tell us about the dynamics of post-seismic deformation?
20 *Geophys. J. Int.* 155, 753–777. doi: 10.1111/j.1365-246X.2003.02030.x.

21 Hill, D. P., Pollitz, F., Newhall, C., 2002. Earthquake-volcano interactions, *Physics Today*, 55,
22 41–47. doi: <http://dx.doi.org/10.1063/1.1535006>.

23 Hirn, A., Nicolich, R., Gallart, J., Laigle, M., Cernobori, L., ETNASEIS Scientific Group
24 (1997), Roots of Etna volcano in faults of great earthquakes, *Earth Planet. Sci. Lett.*, 148, 171–191,
25 doi:10.1016/S0012-821X(97)00023-X.

1 Hyodo, M., Hirahara, K., 2004. GeoFEM Kinematic earthquake cycle simulation in Southwest
2 Japan. *Pure and Applied Geophysics*, 164, 2069-2090. Doi: 10.1007/s00024-004-2549-7.

3 Jaumé, S. C., Sykes, L. R., 1992. Change in the state of stress on the southern San Andreas fault
4 resulting from the California earthquake sequence of April to June 1992. *Science* 258, 1325-1328.
5 doi: 10.1126/science.258.5086.1325.

6 Kagan, Y. Y., 2005. Double-couple earthquake focal mechanism: Random rotation and display,
7 *Geophys. J. Int.*, 163(3), 1065-1072. doi: 10.1111/j.1365-246X.2005.02781.x.

8 Kaverina, A.N., Lander, A.V., Prozorov, A.G., 1996. Global creepex distribution and its relation
9 to earthquake-source geometry and tectonic origin, *Geophys. J. Int.*, 125, 249–265. doi:
10 10.1111/j.1365-246X.1996.tb06549.x.

11 Kenner, S., Segall, P., 1999. Time-dependence of the stress shadowing effect and its relation to
12 the structure of the lower crust. *Geology* 27, 119-122. doi: 10.1130/0091-7613.

13 Kilb, D., Gomber, J., Bodin, P., 2000. Triggering of earthquake aftershocks by dynamic
14 stresses. *Nature*, 408, 570-574. doi:10.1038/35046046.

15 King, G.C.P., Stein R.S., Lin, J., 1994. Static stress changes and the triggering of earthquakes,
16 *Bull. Seismol. Soc. Am.*, 84, 935-953.

17 Marzocchi, W., Casarotti, E., Piersanti, A., 2002. Modeling the stress variations induced by
18 great earthquakes on the largest volcanic eruptions of the 20th century. *Journal of Geophysical*
19 *Research*, 107. doi: 10.1029/2001JB001391.

20 Mattia, M., Patanè, D., Aloisi, M. Amore, M., 2007. Faulting on the western flank of Mt Etna
21 and magma intrusions in the shallow crust. *Terra Nova*, 19, 1-6, doi: 10.1111/j.1365-
22 3121.2006.00724.x.

23 Monaco, C., Catalano, S., Cocina, O., De Guidi, G., Ferlito, C., Gresta, S., Musumeci, C.,
24 Tortorici, L., 2005. Tectonic control on the eruptive dynamics at Mt. Etna volcano (eastern Sicily)
25 during the 2001 and 2002–2003 eruptions, *J. Volcanol. Geotherm. Res.*, 144, 221–233. doi:
26 10.1016/j.jvolgeores.2004.11.024.

1 Monaco, C., De Guidi, G., Ferlito, C., 2011. The morphotectonic map of Mt. Etna, It. J. Geosci.,
2 129, 409–428. doi: 10.3301/IJG.2010.11.

3 Neri, M., Acocella, V., Behncke, B., 2004. The role of the Pernicana Fault System in the
4 spreading of Mt. Etna (Italy) during the 2002–2003 eruption. Bull. Volcanol., 66, 417–430. doi
5 10.1007/s00445-003-0322-x.

6 Neri, M., Acocella, V., Behncke, B., Maiolino, V., Ursino, A., Velardita, R., 2005. Contrasting
7 triggering mechanisms of the 2001 and 2002–2003 eruptions of Mount Etna (Italy). Journal of
8 Volcanology and Geothermal Research, 144, 235-255. doi:10.1016/j.jvolgeores.2004.11.025.

9 Newman, A.V., Dixon, T.H., Ofoegbu, G.I., Dixon, J.E., 2001. Geodetic and seismic constraints
10 on recent activity at Long Valley Caldera, California: evidence for viscoelastic rheology, J.
11 Volcanol. Geotherm. Res., 105, 183–206. [http://dx.doi.org/10.1016/S0377-0273\(00\)00255-9](http://dx.doi.org/10.1016/S0377-0273(00)00255-9).

12 Nostro, C., Stein, R. S., Cocco, M., Belardinelli, M.E., Marzocchi, W., 1998. Two-way coupling
13 between Vesuvius eruptions and southern Apennine earthquakes (Italy) by elastic stress transfer, J.
14 Geophys. Res., 103(B10), 24,487-24,504. doi: 10.1029/98JB00902.

15 Okada, Y., 1992, Internal deformation due to shear and tensile faults in a half-space: Bulletin of
16 the Seismological Society of America, v. 82, no. 2, p. 1018–1040.

17 Palaniyandi Kamatchi, Gunturi Venkata Ramana, Ashok Kumar Nagpal, Nagesh R. Iyer, 2013.
18 Modelling Propagation of Stress Waves through Soil Medium for Ground Response Analysis.
19 Engineering, 5, 611-621. <http://dx.doi.org/10.4236/eng.2013.57073>.

20 Palano, M., Puglisi, G., Gresta S., 2008. Ground deformation patterns at Mt. Etna from 1993 to
21 2000 from joint use of InSAR and GPS techniques, J. Volcanol. Geotherm. Res., 169, 99–120,
22 doi:10.1016/j.jvolgeores.2007.08.014.

23 Palano, M., Gresta, S., Puglisi, G., 2009. Time-dependent deformation of the eastern flank of
24 Mt. Etna: After-slip or viscoelastic relaxation? Tectonophysics, 473, 3-4, 300-311. doi:
25 10.1016/j.tecto.2009.02.047.

1 Patanè, D., Mattia, M., Aloisi, M., 2005. Shallow intrusive processes during 2002-2004 and
2 current volcanic activity on Mt. Etna. *Geophys. Res. Lett.*, 32, p. L06302.
3 <http://dx.doi.org/10.1029/2004GL021773>.

4 Patanè, D., Barberi, G., Cocina, O., De Gori P., Chiarabba, C., 2006. Time-resolved seismic
5 tomography detects magma intrusions at Mount Etna. *Science*, 313, 821. Doi:
6 10.1126/science.1127724.

7 Pavlov, V.F., 1960. The use of the torsional method for determining the viscosity of low melting
8 clays. *Glass Ceram.* 16, 278–283. doi:10.1007/BF00695633.

9 Piombo, A., Tallarico, A., Dragoni, M., 2007. Displacement, strain and stress fields due to shear
10 and tensile dislocations in a viscoelastic half-space. *Geophys. J. Int.*, 170, 1399–1417,
11 doi:10.1111/j.1365-246X.2007.03283.x.

12 Pollitz, F. F., Sacks, I. S., 1997. The 1995 Kobe, Japan, earthquake: A long-delayed aftershock
13 of the offshore 1944 Tonankai and 1946 Nankaido earthquakes. *Bull. Seismol. Soc. Am.* 87, 1-10.

14 Privitera, E., Bonanno, A., Gresta, S., Nunnari, G., Puglisi, G., 2012. Triggering mechanisms of
15 static stress on Mount Etna volcano. An application of the boundary element method. *J. Volcanol.*
16 *Geotherm. Res.*, 245–246 (2012), pp. 149–158. doi:10.1016/j.jvolgeores.2012.08.012.

17 Puglisi, G., Bonforte, A., Ferretti, A., Guglielmino, F., Palano, M., Prati, C., 2008. Dynamics of
18 Mount Etna before, during, and after the July–August 2001 eruption inferred from GPS and
19 differential synthetic aperture radar interferometry data. *Journal of Geophysical Research*, 113,
20 B06405. doi:10.1029/2006JB004811.

21 Reasenber, P.A., Simpson R.W., 1992. Response of regional seismicity to the static stress
22 change produced by the Loma Prieta earthquake, *Science*, 255, 5052, 1687-1690. doi:
23 10.1126/science.255.5052.1687.

24 Resende, R., Lamas, L. N., Lemos, J. V., Calçada, R., 2010. Micromechanical modelling of
25 stress waves in rock and rock fractures. *Rock Mechanics and Rock Engineering*, Volume 43, Issue
26 6, pp 741-761. doi: 10.1007/s00603-010-0098-1.

1 Ruch, J., Pepe, S., Casu, F., Solaro, G., Pepe, A., Acocella, V., Neri, M., Sansosti, E., 2013.
2 Seismo-tectonic behavior of the Pernicana Fault System (Mt Etna): A gauge for volcano flank
3 instability? *Journal of Geophysical Research: Solid Earth*, 118, 4398-4409. doi:10.1002/jgrb.50281.

4 Ryan, M. P., 1987. Neutral buoyancy and the mechanical evolution of magmatic systems, in
5 *Magmatic Processes: Physicochemical Principles*, edited by B. O. Mysen, Spec. Publ. Geochem.
6 Soc., 1, 259–288.

7 Ryan, M. P., 1993. Neutral buoyancy and the structure of mid - ocean ridge magma reservoirs,
8 *J. Geophys. Res.*, 98, 22,321–22,338, doi:10.1029/93JB02394.

9 Ryan, M. P., 1994. Neutral buoyancy - controlled magma transport and storage in mid - ocean
10 ridge magma reservoirs and their sheeted dike complex: A summary of basic relationships, in
11 *Magmatic Systems*, edited by M. P. Ryan, pp. 97–135, Academic, San Diego, Calif..

12 Sevilgen, V., Stein, R. S., Pollitz, F. F., 2012. Stress imparted by the great 2004 Sumatra
13 earthquake shut down transforms and activated rifts up to 400 km away in the Andaman Sea.
14 *PNAS*, 109, 38, 15152-15156. doi:10.1073/pnas.1208799109.

15 Sheu, S.-Y., Shieh, C.F., 2004. Viscoelastic–afterslip concurrence: a possible mechanism in the
16 early post-seismic deformation of the Mw 7.6, 1999 Chi-Chi (Taiwan) earthquake. *Geophys. J. Int.*
17 159, 1112–1124. doi:10.1111/j.1365-246X.2004.02437.x.

18 Singh, S. J., Rosenman, M., 1974. Quasi-static deformation of a viscoelastic half-space by a
19 displacement dislocation. *Physics of the Earth and Planetary Interiors*, 8, 87-101. doi:
20 10.1016/0031-9201(74)90114-9.

21 Spampinato, L., Calvari, S., Oppenheimer, C., Lodato, L., 2008. Shallow magma transport for
22 the 2002–3 Mt. Etna eruption inferred from thermal infrared surveys. *Journal of Volcanology and*
23 *Geothermal Research*, 177, 2, 301-312. doi:10.1016/j.jvolgeores.2008.05.013.

24 Steffke, A. M., Harris, A. J. L., Burton, M., Caltabiano, T., Salerno G. G., Coupled use of
25 COSPEC and satellite measurements to define the volumetric balance during effusive eruptions at

1 Mt. Etna, Italy. *Journal of Volcanology and Geothermal Research*, 205, 47-53.
2 doi:10.1016/j.jvolgeores.2010.06.004.

3 Stein, R. S. 1999. The role of stress transfer in earthquake occurrence, *Nature*, 402, 605-609.
4 doi:10.1038/45144.

5 Thatcher, W., Savage, J.C., 1982. Triggering of large earthquakes by magma-chamber inflation,
6 Izu Peninsula, Japan, *Geology*, 10 (12), 637-640. doi: 10.1130/0091-7613.

7 Toda, S., Stein, R.S., Sagiya, T, 2002. Evidence from the AD 2000 Izu islands earthquake
8 swarm that stressing rate governs seismicity. *Nature* 419, 58–61, doi:10.1038/nature00997.

9 Toda, S., Stein R.S., Lin, J., 2011. Widespread seismicity excitation throughout central Japan
10 following the 2011 M=9.0 Tohoku earthquake and its interpretation by Coulomb stress transfer.
11 *Geophysical Research Letters*, 38, 7. doi: 10.1029/2011GL047834.

12 Trasatti, E., Giunchi, C., Bonafede, M., 2003. Effects of topography and rheological layering on
13 ground deformation in volcanic regions. *Journal of Volcanology and Geothermal Research*, 122, 1-
14 2, 89-110. [http://dx.doi.org/10.1016/S0377-0273\(02\)00473-0](http://dx.doi.org/10.1016/S0377-0273(02)00473-0).

15 Vidale, J., Agnew, D., Oppenheimer, D., Rodriquez, C., Houston, H., 1998. A weak correlation
16 between earthquakes and extensional normal stress and stress rate from lunar tides. *Eos Trans.*
17 *AGU*, 79, Fall Meet. Suppl., F641.

18 Walter, T. R., Amelung, F., 2004. Influence of volcanic activity at Mauna Loa, Hawaii, on
19 earthquake occurrence in the Kaoiki Seismic Zone, *Geophys. Res. Lett.*, 31, L07622,
20 doi:10.1029/2003GL019131.

21 Walter, T. R., Acocella, V., Neri, M., Amelung, F., 2005. Feedback processes between
22 magmatic events and flank movement at Mount Etna (Italy) during the 2002–2003 eruption, *J.*
23 *Geophys. Res.*, 110, B10205. doi:10.1029/2005JB003688.

Figure 1

[Click here to download Figure: figure1.pdf](#)

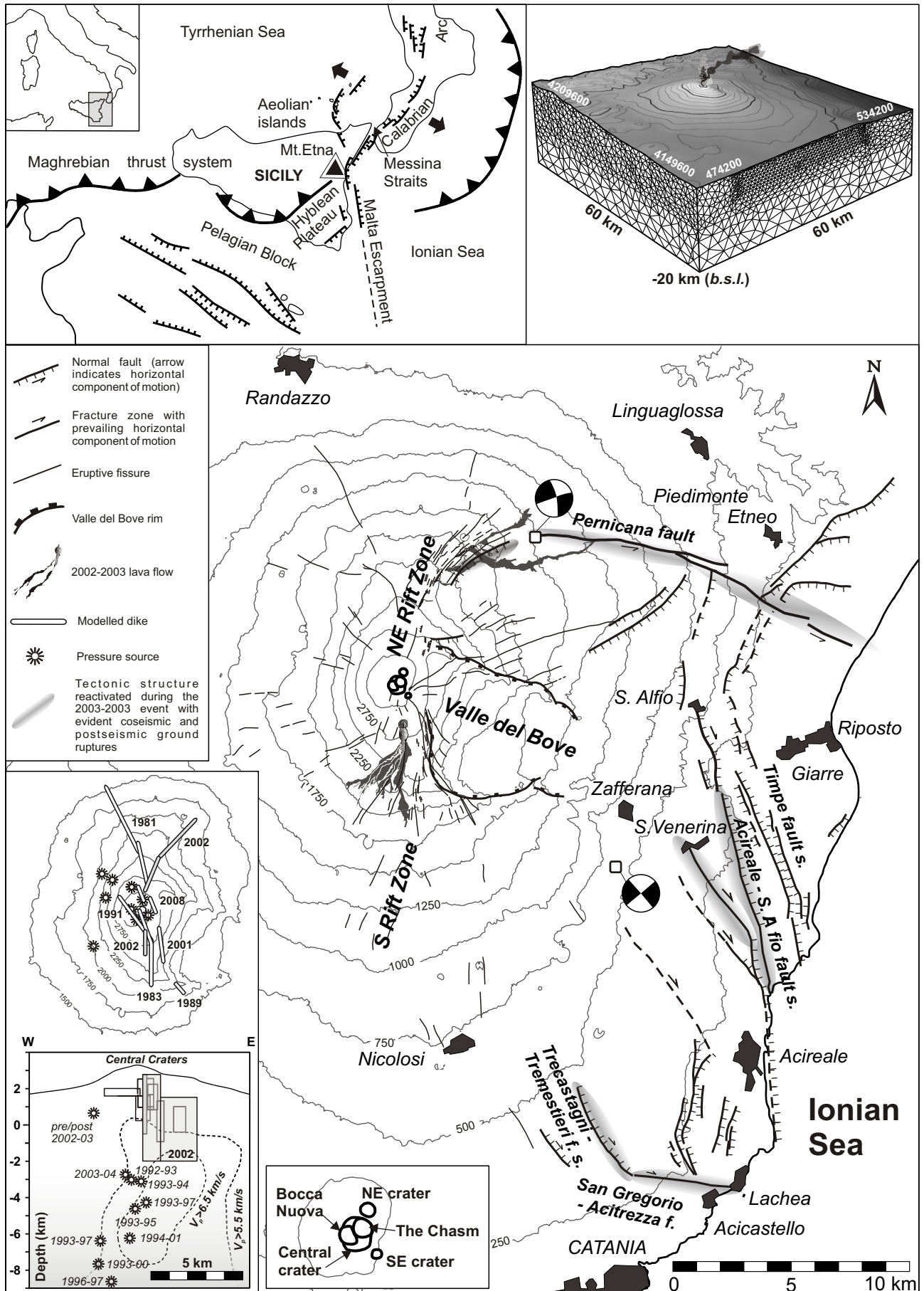


Figure 2
[Click here to download Figure: figure2.pdf](#)

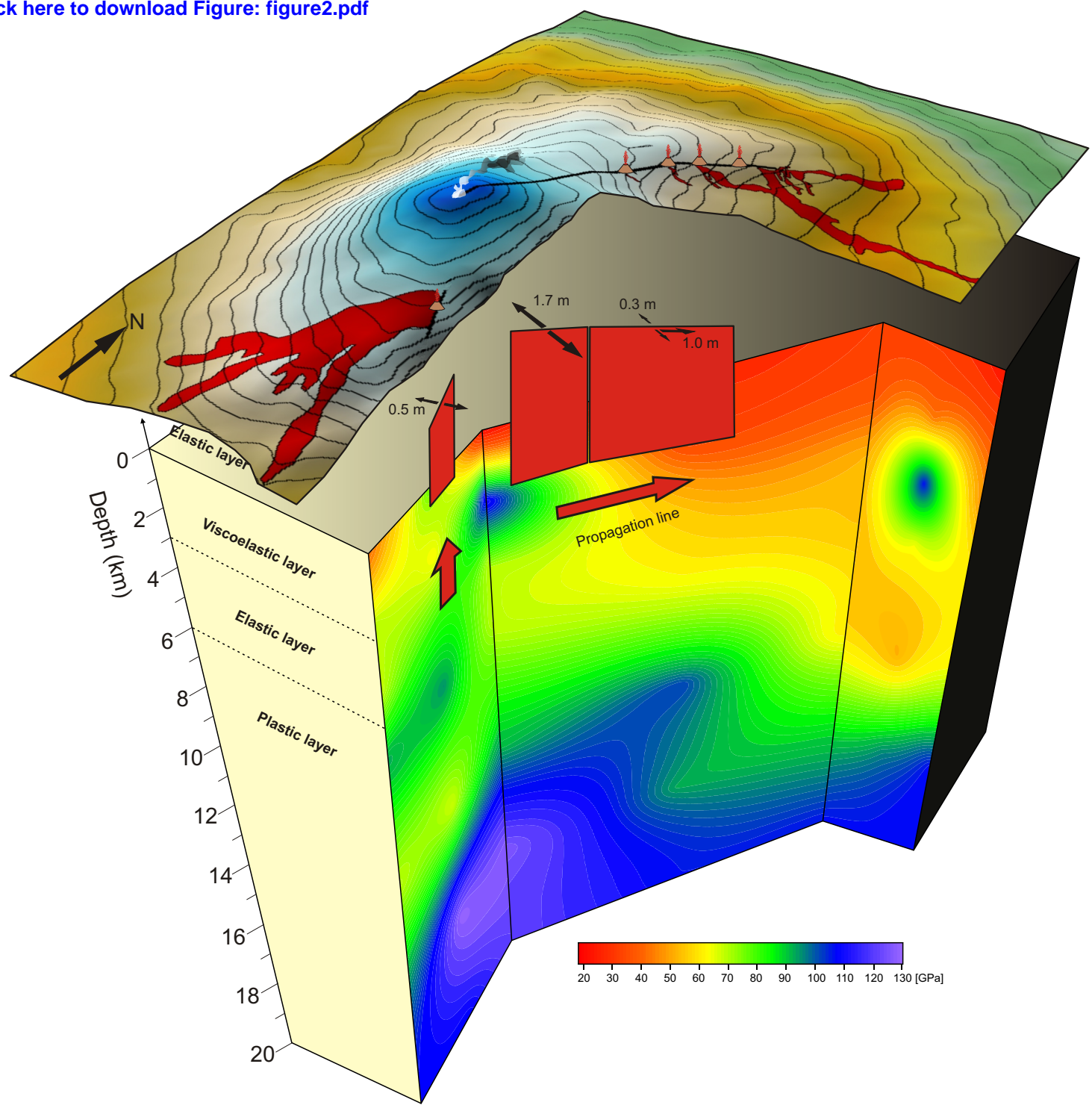


Figure 3

[Click here to download Figure: figure3.pdf](#)

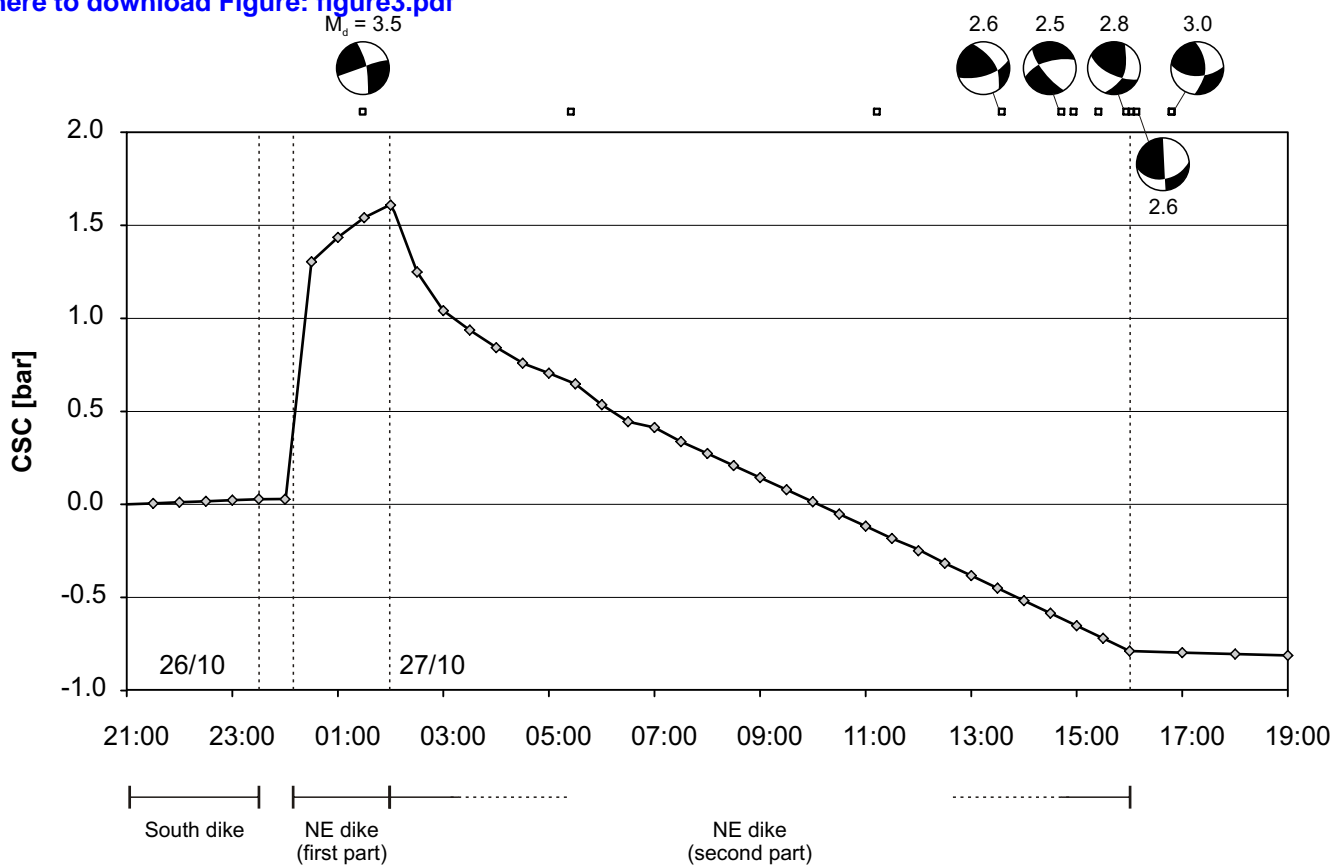


Figure 4
[Click here to download Figure: figure4.pdf](#)

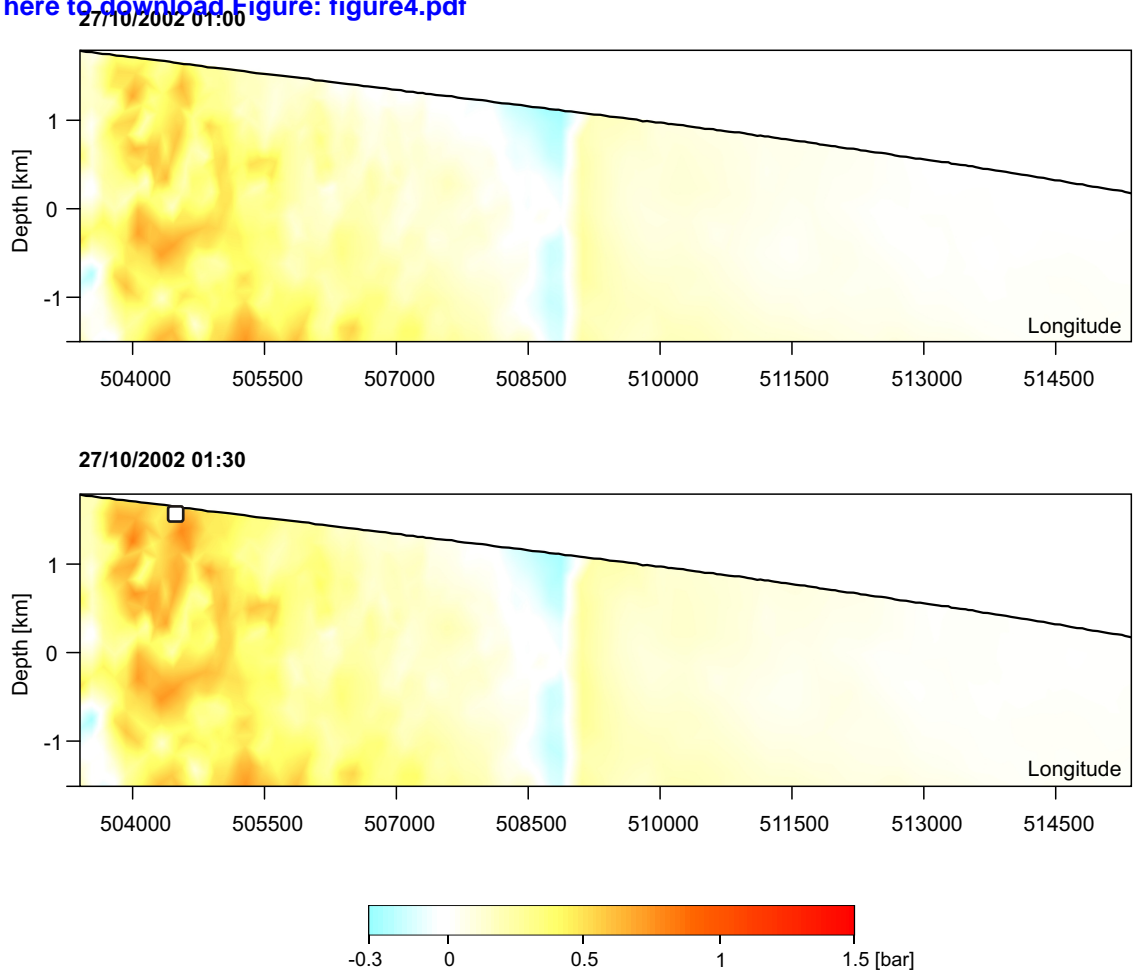


Figure 5

[Click here to download Figure: figure5.pdf](#)

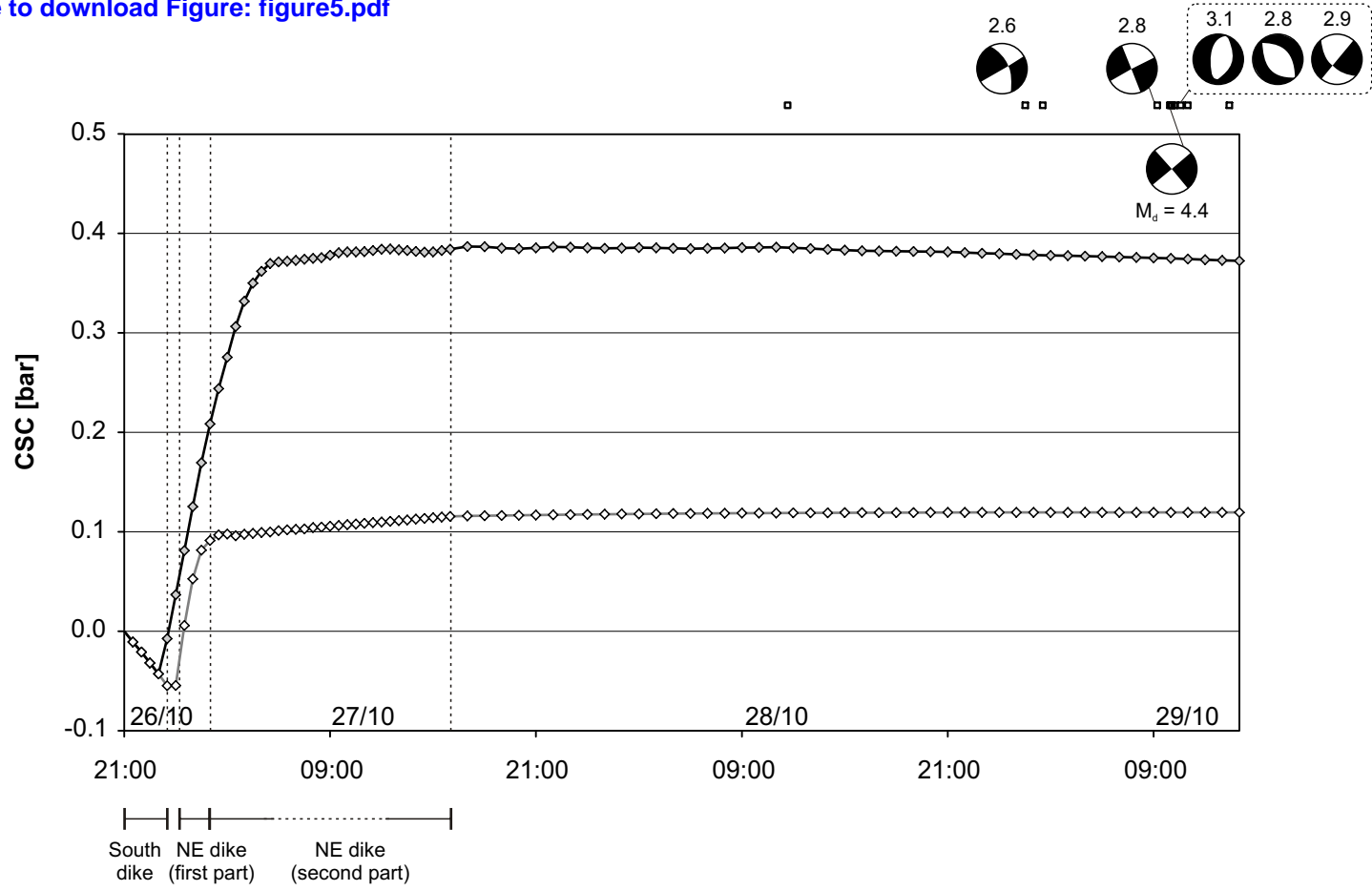


Figure 6

[Click here to download Figure: figure6.pdf](#)

